

Intrinsic anomalous Hall effect in nickel: An GGA+U study

Huei-Ru Fuh and Guang-Yu Guo*

*Department of Physics and Center for Theoretical Sciences,
National Taiwan University, Taipei 10617, Taiwan and*

Graduate Institute of Applied Physics, National Chengchi University, Taipei 11605, Taiwan

(Dated: June 24, 2021)

The electronic structure and intrinsic anomalous Hall conductivity of nickel have been calculated based on the generalized gradient approximation (GGA) plus on-site Coulomb interaction (GGA+U) scheme. The highly accurate all-electron full-potential linearized augmented plane wave method is used. It is found that the intrinsic anomalous Hall conductivity (σ_{xy}^H) obtained from the GGA+U calculations with $U = 1.9$ eV and $J = 1.2$ eV, is in nearly perfect agreement with that measured recently at low temperatures while, in contrast, the σ_{xy}^H from the GGA calculations is about 100 % larger than the measured one. This indicates that, as for the other spin-orbit interaction (SOI)-induced phenomena in 3d itinerant magnets such as the orbital magnetic magnetization and magnetocrystalline anisotropy, the on-site electron-electron correlation, though moderate only, should be taken into account properly in order to get the correct anomalous Hall conductivity. The intrinsic σ_{xy}^H and the number of valence electrons (N_e) have also been calculated as a function of the Fermi energy (E_F). A sign change is predicted at $E_F = -0.38$ eV ($N_e = 9.57$), and this explains qualitatively why the theoretical and experimental σ_{xy}^H values for Fe and Co are positive. It is also predicted that fcc $\text{Ni}_{(1-x)}\text{Co}(\text{Fe,Cu})_x$ alloys with x being small, would also have the negative σ_{xy}^H with the magnitude being in the range of $500 \sim 1400 \Omega^{-1}\text{cm}^{-1}$. The most pronounced effect of including the on-site Coulomb interaction is that all the d -dominant bands are lowered in energy relative to the E_F by about 0.3 eV, and consequently, the small minority spin X_2 hole pocket disappears. The presence of the small X_2 hole pocket in the GGA calculations is attributed to be responsible for the large discrepancy in the σ_{xy}^H between theory and experiment.

PACS numbers: 71.15.Mb, 71.70.Ej, 72.15.Gd, 75.47.Nb

I. INTRODUCTION

Anomalous Hall effect (AHE) refers to the transverse charge current generation in solids in a ferromagnetic phase by the electric field and has received intensive renewed interest in recent years mainly because of its close connection with spin transport phenomena[1]. There are several competing mechanisms proposed for the AHE. Extrinsic mechanisms of skew scattering[2] and side jump[3] refer to the modified impurity scattering caused by the spin-orbit interaction (SOI). Another mechanism arises from the transverse velocity of the Bloch electrons induced by the SOI, discovered by Karplus and Luttinger[4], and thus is of intrinsic nature. This intrinsic AHE has recently been reinterpreted in terms of the Berry curvature of the occupied Bloch states.[5–8] Furthermore, recent quantitative first-principles studies based on the Berry phase formalism showed that the intrinsic AHE is important in various materials.[9] In particular, in itinerant ferromagnets such as Fe and Co, the intrinsic anomalous Hall conductivity given by first-principles calculations[9, 10] has been found to agree with the experimental anomalous Hall conductivity [11–13] within 30 %, thereby demonstrating the dominance of the intrinsic mechanism. Nonetheless, the physical origin of the AHE in nickel is still not fully understood. Re-

cent first-principles density functional calculations with the generalized gradient approximation (GGA) predicted a large intrinsic anomalous Hall conductivity of $-2203 \Omega^{-1}\text{cm}^{-1}$ in Ni[10], which is more than three times larger than the corresponding experimental value of $-646 \Omega^{-1}\text{cm}^{-1}$ [14] at room temperature. In the latest experiment[15], the intrinsic Hall conductivity was found to be $-1100 \Omega^{-1}\text{cm}^{-1}$ at low temperatures. Though this value is significantly larger than that of the much earlier experiment[14], it is still only half of the calculated intrinsic Hall conductivity[10].

First-principles GGA calculations have been rather successful in describing many physical properties such as crystal structure, elastic constant and spin magnetic moment, of itinerant ferromagnets Fe, Co and Ni (see, e.g., Ref. 16 and references therein). However, GGA calculations fail in describing some relativistic SOI-induced phenomena in these itinerant magnets. For example, the theoretical values of orbital magnetic moment account for only about 50 % of the measured ones in Fe and Co[17] and the calculated magnetocrystalline anisotropy energy of Ni is even wrong in sign[18]. This failure of the GGA is generally attributed to its incorrect treatment of the moderate 3d electron-electron correlation in these systems. Several theoretical methods that go beyond the density functional theory (DFT) with the local density approximation (LDA) or GGA, such as the orbital-polarization correction[19] and LDA/GGA plus on-site Coulomb interaction U (LDA/GGA+U)[20–22] schemes, have been developed for better description of

* gyguo@phys.ntu.edu.tw

the SOI-induced phenomena in magnetic solids. Indeed, the orbital-polarization correction has been found to bring the calculated orbital moments in many itinerant magnets such as Fe and Co in good agreement with experiments[17]. Furthermore, it has been demonstrated that the correct easy axes and the magnitudes of the magnetocrystalline anisotropy energy of Fe and Ni can be obtained within the LDA+U scheme.[23]

Therefore, in this work, we perform GGA+U calculations for nickel to better understand the mechanism of its anomalous Hall effect. We use highly accurate all-electron full-potential linearized augmented plane wave (FLAPW) method[24]. We find that including on-site electron-electron correlation in nickel has significant effect on its anomalous Hall effect as well as its electronic structure near the Fermi level. In particular, the calculated anomalous Hall conductivity reduces from $-2200 \Omega^{-1}\text{cm}^{-1}$ (GGA) to $-1066 \Omega^{-1}\text{cm}^{-1}$, and the latter value is in very good agreement with the measured low temperature intrinsic Hall conductivity of $-1100 \Omega^{-1}\text{cm}^{-1}$ from latest experiments.[15]

This paper is organized as follows. In next section, we briefly describe how the intrinsic anomalous Hall conductivity is calculated within the linear-response Kubo formalism as well as the numerical method and computational details used in the present work. In Sec. III, we first present the calculated anomalous Hall conductivity, magnetic moments and also relativistic band structure. We then compare our results with available experiments and also previous calculations. Finally, we make some predictions about the intrinsic anomalous Hall conductivity for fcc $\text{Ni}_{(1-x)}\text{Co}(\text{Fe,Cu})_x$ alloys with small Co(Fe,Cu) concentration x , within the rigid band approximation. In Sec. IV, we summarize the main conclusions drawn from the present work.

II. THEORY AND COMPUTATIONAL DETAILS

The intrinsic anomalous Hall conductivity of a solid can be evaluated by using the Kubo formula [25]. The intrinsic Hall effect comes from the static limit ($\omega=0$) of the off-diagonal element of the optical conductivity [25, 26]. Following the procedure for the calculation of the intrinsic spin Hall conductivity[26], we first calculate the imaginary part of the off-diagonal element of the optical conductivity

$$\begin{aligned} \sigma_{xy}^{(2)}(\omega) = & \frac{\pi e^2}{\omega V_c} \sum_{\mathbf{k}} \sum_{n \neq n'} (f_{\mathbf{k}n} - f_{\mathbf{k}n'}) \text{Im}[\langle \mathbf{k}n | v_x | \mathbf{k}n' \rangle \\ & \times \langle \mathbf{k}n | v_y | \mathbf{k}n' \rangle] \delta(\hbar\omega - \epsilon_{n'n}) \end{aligned} \quad (1)$$

where V_c is the unit cell volume, $\hbar\omega$ is the photon energy, $|\mathbf{k}n\rangle$ is the n th Bloch state with crystal momentum \mathbf{k} , $v_{x(y)}$ is the velocity operator, and $\epsilon_{n'n} = \epsilon_{\mathbf{k}n'} - \epsilon_{\mathbf{k}n}$. We

then obtain the real part from the imaginary part by a Kramers-Kronig transformation

$$\sigma_{xy}^{(1)}(\omega) = -\frac{2}{\pi} \mathbf{P} \int_0^\infty d\omega' \frac{\omega' \sigma_{xy}^{(2)}(\omega')}{\omega'^2 - \omega^2} \quad (2)$$

where \mathbf{P} denotes the principle value of the integral. The intrinsic anomalous Hall conductivity σ_{xy}^H is the static limit of the off-diagonal element of the optical conductivity $\sigma_{xy}^{(1)}(\omega=0)$. We notice that the anomalous Hall conductivity of bcc Fe calculated in this way[9, 27] is in quantitative agreement with that calculated directly by accounting for the Berry phase correction to the group velocity [9].

Since all the intrinsic Hall effects are caused by the SOI, first-principles calculations must be based on a relativistic band theory. Here the relativistic band structure of fcc Ni is calculated using the highly accurate FLAPW method, as implemented in the WIEN2K code[28]. The self-consistent electronic structure calculations are based on the DFT with the GGA for the exchange correlation potential [29]. To further take d -electron correlation into account, we include on-site Coulomb interaction U in the GGA+U approach[20]. The so-called around-mean-field (AMF) scheme for double counting correction[22] is adopted here. $U = 1.9$ eV and $J = 1.2$ eV, which were found to give the correct sign and magnitude of magnetocrystalline anisotropy energy for fcc Ni[23], are used. Furthermore, the GGA+U calculations using the double counting correction scheme designed for approximate self-interaction correction (SIC) for strongly correlated systems such as transition metal oxides[21], have also been performed. Nevertheless, the theoretical anomalous Hall conductivities from the GGA+U calculations using both double counting correction schemes, are almost identical (see Table I below). Since the AMF scheme is believed to be more suitable for metallic systems[22], here we will concentrate on the results of the AMF calculations. Moreover, the GGA+U calculations with a larger U value of 2.5 eV are also performed to see how the variation of U may affect the calculated anomalous Hall conductivity.

The experimental lattice constant $a = 3.52 \text{ \AA}$ [30] is used here. The muffin-tin sphere radius (R_{mt}) used is 2.2 a.u. The wave function, charge density, and potential were expanded in terms of the spherical harmonics inside the muffin-tin spheres, and the cutoff angular momentum (L_{max}) used is 10, 6, and 6, respectively. The wave function outside the muffin-tin spheres was expanded in terms of the augmented plane waves, and a large number of augmented plane waves (about 70 APWs per atom, i.e., the maximum size of the crystal momentum $K_{max} = 8/R_{mt}$) were included in the present calculations. The improved tetrahedron method is used for the Brillouin-zone integration.[31] To obtain accurate ground state charge density as well as spin and orbital magnetic moments, a fine $56 \times 56 \times 56$ grid of 185193 k -points in the first Brillouin zone was used.

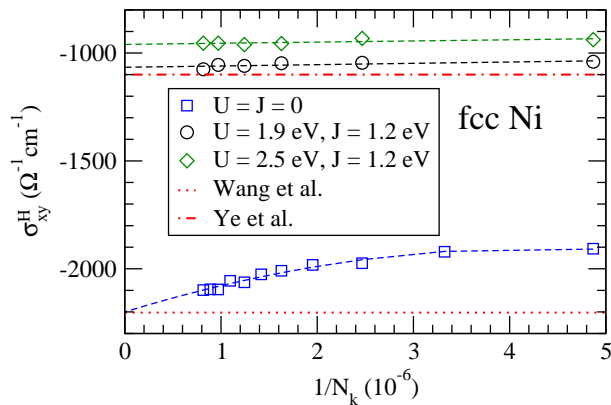


FIG. 1. (Color online) Calculated anomalous Hall conductivity σ_{xy}^H as a function of the inverse of the number of k -points in the Brillouin zone (N_k). The dashed lines are a polynomial fit to the calculated values to get the extrapolated value of σ_{xy}^H at $N_k = \infty$. For comparison, the theoretical value by Wang *et al.*[10] and the experimental value by Ye *et al.*[15] are also shown as the horizontal dotted and dot-dashed lines, respectively.

III. RESULTS AND DISCUSSION

Like the calculation of the magnetocrystalline anisotropy energy of bulk magnets[18], a very fine k -point mesh is needed for the anomalous Hall conductivity calculation.[9, 10] Therefore, we perform the σ_{xy}^H calculations using several extremely fine k -point meshes with the finest k -point mesh being $106 \times 106 \times 106$. The calculated σ_{xy}^H is plotted as a function of the inverse of the number (N_k) of k -points in the first Brillouin zone in Fig. 1. The calculated values of σ_{xy}^H are fitted to a polynomial to get the converged theoretical σ_{xy}^H (i.e., the extrapolated value of σ_{xy}^H at $N_k = \infty$) (see Fig. 1). The theoretical σ_{xy}^H obtained in this way as well as the calculated spin (m_s) and orbital (m_o) magnetic moments are listed in Table I. Also listed in Table I are the available experimental and previous theoretical σ_{xy}^H , m_s and m_o .

Table I shows that the theoretical σ_{xy}^H from the GGA is $-2200 \Omega^{-1}\text{cm}^{-1}$, and is much larger than the experimental value of $-646 \Omega^{-1}\text{cm}^{-1}$ at room temperature[14] and also the experimentally derived intrinsic value of $-1100 \Omega^{-1}\text{cm}^{-1}$ at low temperatures[15]. Nevertheless, the present result is in very good agreement with the previous GGA calculations[10], as it should be (see Table I and Fig. 1). Interestingly, when the on-site Coulomb interaction is taken into account via the GGA+U scheme, the calculated σ_{xy}^H reduces significantly. In particular, when $U = 1.9 \text{ eV}$ and $J = 1.2 \text{ eV}$ which were found to give rise to the correct easy axis and magnitude of the magnetocrystalline anisotropy energy[23], the theoretical σ_{xy}^H becomes $-1066 \Omega^{-1}\text{cm}^{-1}$. This good agreement between the present GGA+U calculation and the low temperature measurements[15] (Table I and Fig. 1) indicates that the intrinsic AHE dominates in nickel and

TABLE I. Calculated anomalous Hall conductivity σ_{xy}^H ($\Omega^{-1}\text{cm}^{-1}$) as well as spin magnetic moment m_s (μ_B/atom) and orbital magnetic moment m_o (μ_B/atom). Superscripts of SIC indicate that the values are obtained from the GGA+U calculations with the SIC double counting correction scheme (see Sec. II). The corresponding experimental values as well as previous theoretical σ_{xy}^H are also listed for comparison.

	GGA	GGA+U U=1.9eV	GGA+U U=2.5eV	Expt.
σ_{xy}^H	-2200 -2203 ^b	-1066 -1107 ^{SIC}	-960 -945 ^{SIC}	-646 ^a -1100 ^c
m_s	0.639	0.661 0.685 ^{SIC}	0.675 0.707 ^{SIC}	0.57 ^d
m_o	0.051	0.066 0.069 ^{SIC}	0.071 0.076 ^{SIC}	0.05 ^d

^aReference 14.

^bReference 10.

^cReference 15.

^dReference 32.

that the $3d$ electron-electron correlation in itinerant magnets such as nickel has an important effect on the AHE, although being only moderate. Further increasing U to 2.5 eV reduces the calculated σ_{xy}^H slightly (Table I and Fig. 1). As expected, the GGA+U calculations increase the theoretical spin and orbital magnetic moments, and hence enlarge somewhat the discrepancies between the calculations and experiments (Table I). Nonetheless, with $U = 1.9 \text{ eV}$ and $J = 1.2 \text{ eV}$, the theoretical spin and orbital magnetic moments are still in reasonable agreement with the experiments (Table I).

To help understand how the on-site electron-electron correlation affects the electronic band structure and AHE in nickel, we plot in Fig. 2 and Fig. 3 the relativistic energy bands along the high symmetry lines in the Brillouin zone calculated both without and with on-site Coulomb interaction U . The relativistic band structure may be regarded as the result of a superposition of the corresponding scalar-relativistic spin-up and spin-down band structures with many accidental band-crossings (degeneracies) lifted by the SOI. In nickel, nevertheless, these SOI-induced splittings are generally much smaller than the exchange splittings, and thus can be treated as a perturbation.[33] Also, including the SOI would lower the symmetry of the system. In the present work, the magnetization is assumed to be along the $[001]$ direction, and the symmetry of the system becomes the tetragonal one. The six high symmetry X points which are equivalent in the nonrelativistic (or scalar-relativistic) case, now form two inequivalent groups, namely, two equivalent $\pm Z$ points and four equivalent $\pm X$ and $\pm Y$ points. Therefore, the energy bands near the Z point are slightly different from that near the X and Y points, as shown in Fig. 2 and Fig. 3. The relativistic band structure and Fermi surface of Ni has been reported by several researchers before by using different band structure calculation methods (see, e.g., Refs. 10, 18, 23, and 33). In

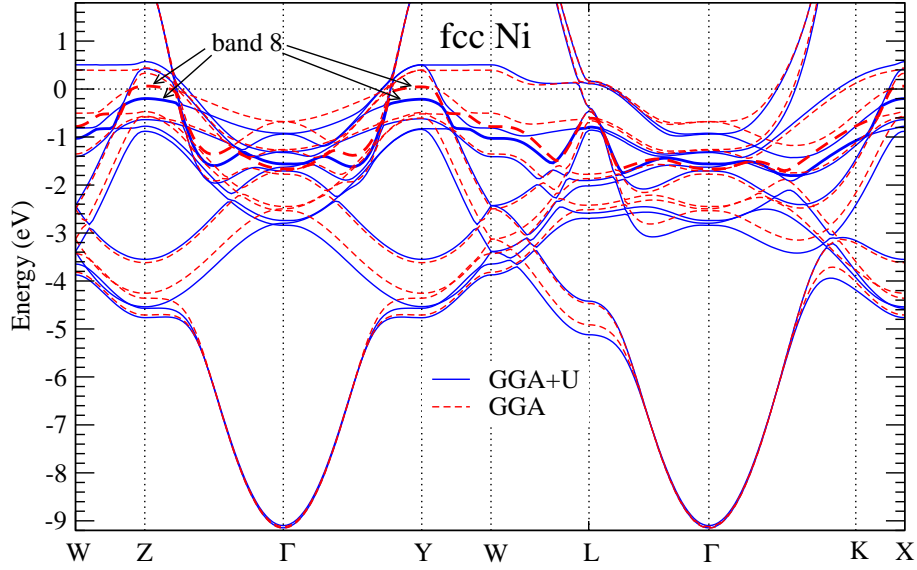


FIG. 2. (Color online) Relativistic GGA and GGA+U band structures. The GGA+U band structure was obtained using $U = 1.9$ eV and $J = 1.2$ eV. The Fermi level (dotted horizontal line) is at 0 eV. The thick curves denote band 8's which are also indicated by the arrowed lines.

particular, Wang and Callaway analysed in detail the energy band characters and Fermi surface sheets.[33] The present GGA relativistic band structure (the red dashed curves in Fig. 2 and Fig. 3) is very similar to that reported by Wang and Callaway[33]. For example, in both cases, there are five bands (bands 8-12) crossing the Fermi level, and there is a small down-spin-dominant hole pocket (band 8, noted as X_2) centered at the X(Y,Z) symmetry point (see Figs. 2-3, and also Fig. 1 in Ref. 33). However, the small X_2 hole pocket was not found in the de Haas-van Alphen experiments.[34]

Now let us focus on the changes in the relativistic band structure caused by including the on-site Coulomb interaction. A pronounced change is that all the d -dominant bands are lowered in energy relative to the Fermi level, when the on-site Coulomb interaction is taken into account in the GGA+U scheme (see Figs. 2-3). In other words, the binding energy of the d -dominated valence bands is increased by about 0.3 eV. In particular, the down-spin band 8 is now pushed completely below the Fermi level and the small X_2 hole pocket disappears. The absence of the X_2 hole pocket is consistent with the de Haas-van Alphen experiments.[34] In Ref. 23, the absence of the X_2 hole pocket caused by the on-site Coulomb interaction was regarded as the main reason that the LDA+U calculations predicted the correct easy axis for nickel. As will be shown below, this band 8 near the Fermi level calculated without the on-site Coulomb interaction, gives rise to a pronounced contribution to the anomalous Hall conductivity, and thus the absence of the small X_2 hole pocket in the GGA+U band structure is also the main cause for the significant reduction of the calculated anomalous Hall conductivity.

In Fig. 3, we display the anomalous Hall conductivity

(σ_{xy}^H) and the number of valence electrons (N_e) as a function of the Fermi level (E_F), together with the relativistic band structure, from the GGA+U calculations using $U = 1.9$ eV and $J = 1.2$ eV. The fine k -point mesh of $106 \times 106 \times 106$ is used. Clearly, the magnitude of the σ_{xy}^H peaks just above the true Fermi level ($E_F = 0$ eV), with a large value of $-1420 \Omega^{-1}\text{cm}^{-1}$ at 0.16 eV ($N_e \approx 10.3$). The peak may be related to the flat band (band 10) along the W-L- Γ line near the L point just above the Fermi level (see Fig. 3a). As the Fermi level is further artificially raised, the size of the σ_{xy}^H decreases steadily and becomes rather small (within $200 \Omega^{-1}\text{cm}^{-1}$) above 0.75 eV. When the E_F is artificially lowered, the magnitude of the σ_{xy}^H initially decreases gradually, and then drops sharply starting at $E_F = -0.35$ eV. The resultant shoulder at -0.35 eV can be attributed to the presence of the top segment of band 8 near the X (Y,Z) point in this energy region (see Fig. 3a). The σ_{xy}^H then changes its sign at -0.38 eV (or $N_e \approx 9.57$). As the E_F is further lowered, the σ_{xy}^H increases sharply and then peaks at -0.74 eV (or $N_e \approx 8.90$) with a large value of $2635 \Omega^{-1}\text{cm}^{-1}$. Beyond this point, the σ_{xy}^H decreases and fluctuates but remains positive as the E_F is further lowered, and it then changes its sign again at -2.28 eV (or $N_e \approx 4.78$). For the E_F being below -3.80 eV, the magnitude of the σ_{xy}^H is small. Note that the energy bands below -4.0 eV and above 0.5 eV are predominantly of $4s4p$ character and thus the effects of the SOI and exchange interaction are small.

Experimentally, the measured anomalous Hall resistivity ρ_{xy} is often analyzed in terms of two distinctly different resistivity (ρ_{xx})-dependent terms[1], i.e., $\rho_{xy} = a\rho_{xx} + b\rho_{xx}^2$. Since usually $\rho_{xy} \ll \rho_{xx}$, the total anomalous Hall conductivity $\sigma_{xy} = -\rho_{xy}/(\rho_{xy}^2 + \rho_{xx}^2) \approx a\sigma_{xx} + b$,

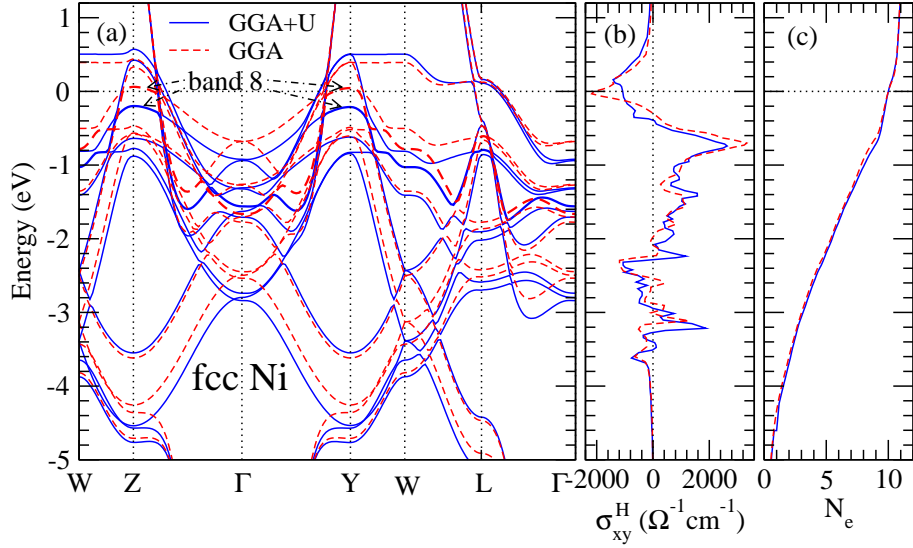


FIG. 3. (Color online) Relativistic band structure (a), anomalous Hall conductivity (σ_{xy}^H) (b), and number of valence electrons (N_e) (c), calculated with (solid blue lines) and without (dashed red lines) on-site Coulomb interaction U . Both σ_{xy}^H and N_e were calculated using the fine k -point mesh of $106 \times 106 \times 106$. The GGA+U results were obtained using $U = 1.9$ eV and $J = 1.2$ eV. The Fermi level (dotted horizontal line) is at 0 eV. In (a), the thick curves denote band 8's which are also indicated by the arrowed lines.

where the first linear σ_{xx} -dependent term ($a\sigma_{xx}$) was attributed to the extrinsic skew scattering mechanism (σ_{xy}^{SK}) [2]. The skew scattering contribution has been found to become dominant in dilute impurity metals at low temperatures. [1] Indeed, recent *ab initio* calculations for the alloy systems $\text{Fe}_{1-x}\text{Pd}_x$ and $\text{Ni}_{1-x}\text{Pd}_x$ indicated that in the small Pd concentration x region, the σ_{xy}^{SK} can be several times larger than the b , and can also differ in sign. [35] The second scattering-independent term b was usually further separated into the intrinsic contribution σ_{xy}^H [4] which can be obtained from band structure calculations [1], as done here for nickel, and also the extrinsic side jump mechanism (σ_{xy}^{SJ}) [3]. Therefore, when one compares the calculated σ_{xy}^H with the experimental scattering-independent term b , one should be aware of the possible side jump contribution σ_{xy}^{SJ} even though it has been shown that the σ_{xy}^H would dominate in ferromagnet metals such as Fe and Co [9, 10]. Recent theoretical calculations for the 2D Rashba and 3D Luttinger Hamiltonians using a Gaussian disorder model potential suggested that the AHE in the (III,Mn)V ferromagnetic semiconductors at low temperatures could be dominated by the σ_{xy}^{SJ} . [36] However, more recent *ab initio* calculations show that in fcc $\text{Fe}_{1-x}\text{Pd}_x$ and $\text{Ni}_{1-x}\text{Pd}_x$, the σ_{xy}^{SJ} is generally two-order of magnitude smaller than both the σ_{xy}^{SK} and σ_{xy}^H , thus being negligible. [35] This is consistent with the recent experimental finding of the negligible σ_{xy}^{SJ} in bcc Fe [13] and fcc Ni [15] using a newly established empirical σ_{xx} -scaling formula for σ_{xy} [13].

Let us now return to the calculated σ_{xy}^H as a function of the E_F described above and also presented in Fig. 3. We find that it can explain qualitatively within the

rigid band approximation the known AHE experiments on 3d transition metal ferromagnets and their alloys. [11–14] For example, the sign of the σ_{xy}^H of both Fe and Co were found to be positive. [11–13] Interestingly, the calculated σ_{xy}^H at $N_e = 8.0$ ($E_F = -1.02$ eV) is $758 \Omega^{-1}\text{cm}^{-1}$, being in very good agreement with the previous *ab initio* calculations for Fe [9]. Of course, this nearly perfect agreement may be accidental because Fe crystallizes in the bcc structure and also has a much larger spin magnetic moment, and hence the rigid band model should not work very well here. We note that the calculated σ_{xy}^H is $2548 \Omega^{-1}\text{cm}^{-1}$ at $N_e = 9.0$ ($E_F = -0.71$ eV), which is much larger than the previous theoretical σ_{xy}^H value for fcc Co [37] and also the experimental σ_{xy}^H value for polycrystalline hcp Co [38]. Nickel forms substitutional alloys in fcc structure with low concentration of Fe, Co and Cu. The present calculations (Fig. 3) predict that fcc $\text{Ni}_{(1-x)}\text{Co}(\text{Fe,Cu})_x$ alloys (x being small) would have the negative intrinsic σ_{xy}^H with the magnitude being in the range of $500 \sim 1400 \Omega^{-1}\text{cm}^{-1}$. Of course, when comparing this prediction with the AHE experiments on fcc $\text{Ni}_{(1-x)}\text{Co}(\text{Fe,Cu})_x$ alloys, one should take into account the non-negligible skew scattering contribution σ_{xy}^{SK} [35]. Indeed, as mentioned earlier, Fig. 3b shows a sign change of σ_{xy}^H at $N_e \approx 9.570$ ($E_F = -0.38$ eV), whereas the sign change of the σ_{xy} in fcc $\text{Ni}_{1-x}\text{Fe}_x$ alloys with $x \approx 0.13$ (i.e., $N_e \approx 9.74$) was experimentally found [2]. This experimentally found sign change at the lower Fe concentration could be attributed to the presence of the positive σ_{xy}^{SK} in fcc $\text{Ni}_{1-x}\text{Fe}_x$ alloys.

As mentioned before, the most pronounced effect of including the on-site Coulomb interaction is that all the

d -dominant bands are lowered in energy relative to the E_F by about 0.3 eV. Consequently, the down-spin band 8 is now pushed completely below the E_F and the small X_2 hole pocket disappears. Now the top of band 8 is located at -0.20 eV on the X(Y,Z) point (Figs. 2-3). To see clearly the effect of the on-site Coulomb interaction on the σ_{xy}^H , we also display in Fig. 3 the anomalous Hall conductivity (σ_{xy}^H) and the number of valence electrons (N_e) as a function of E_F , together with the relativistic band structure, from the GGA calculations using the fine k -point mesh of $106 \times 106 \times 106$. Strikingly, the σ_{xy}^H exhibits a pronounced negative peak right at the E_F with the value being about $-2178 \Omega^{-1}\text{cm}^{-1}$ (see Fig. 3b). The remarkable difference in the σ_{xy}^H at 0.0 eV from the GGA and GGA+U calculations can be attributed to the presence of the above mentioned X_2 hole pocket in the GGA calculation (Fig. 3). Another major difference is the absence of the clear shoulder at -0.35 eV in the GGA σ_{xy}^H spectrum. This is because of the absence of the top segment of band 8 near the X (Y,Z) point in this energy region in the GGA band structure (see Fig. 3a). In fact, Fig. 3 shows that as the E_F is lowered from the true Fermi level (0 eV), the GGA σ_{xy}^H decreases in magnitude steeply to zero and changes its sign at -0.30 eV ($N_e = 9.55$). Nevertheless, in both cases, the σ_{xy}^H changes its sign near $N_e = 9.56$. The other pronounced difference (by about $700 \Omega^{-1}\text{cm}^{-1}$) in the two calculated σ_{xy}^H spectra is the height of the positive peak near -0.70 eV. In the rest of the energy region, the two σ_{xy}^H spectra look rather similar.

IV. CONCLUSIONS

In summary, we have calculated the electronic structure and intrinsic anomalous Hall conductivity of nickel with both the GGA and GGA+U schemes. The highly accurate all-electron FLAPW method is used. We find that the theoretical anomalous Hall conductivity (σ_{xy}^H) obtained from the GGA calculations (Table I) is about 100 % larger than the intrinsic σ_{xy}^H recently measured at

low temperatures[15]. In contrast, the theoretical σ_{xy}^H from the GGA+U calculations with $U = 1.9$ eV and $J = 1.2$ eV is in almost perfect agreement with the measured one (Table I). This indicates that, as for other SOI-induced magnetic phenomena in 3d itinerant magnets such as the orbital magnetic magnetization and magnetocrystalline anisotropy, the on-site electron-electron correlation, though moderate only, should be taken into account properly in order to get the correct anomalous Hall conductivity. The most significant effect of including the on-site Coulomb interaction is that all the d -dominant bands are lowered in energy relative to the E_F by about 0.3 eV. Consequently, the down-spin band 8 is now pushed completely below the E_F and the small X_2 hole pocket disappears. The presence of the small X_2 hole pocket in the LDA and GGA calculations is found to be the main reason why the large discrepancy in the σ_{xy}^H between theory and experiment exists. The intrinsic anomalous Hall conductivity (σ_{xy}^H) has also been calculated as a function of the Fermi level E_F (or the number of valence electrons N_e) in the GGA+U scheme. A sign change is predicted at $E_F = -0.38$ eV (or $N_e = 9.57$), and this explain qualitatively why the theoretical and experimental σ_{xy}^H values for Fe and Co are positive. Finally, the present calculations (Fig. 3) indicate that fcc $\text{Ni}_{(1-x)}\text{Co}(\text{Fe,Cu})_x$ alloys (x being small) would also have the negative intrinsic σ_{xy}^H with the magnitude being in the range of $500 \sim 1400 \Omega^{-1}\text{cm}^{-1}$.

ACKNOWLEDGMENTS

G.Y.G thanks Xiaofeng Jin for communicating their experimental results[15] prior to the submission for publication. The authors acknowledge the supports from the National Science Council and NCTS of Taiwan. Some calculations were carried out on the computers at the National Center for High-Performance Computing of Taiwan.

-
- [1] N. Nagaosa, J. Sinova, S. Onoda, A. H. MacDonald, and N. P. Ong, Rev. Mod. Phys. **82**, 1539 (2010)
 - [2] J. Smit, Physica (Amsterdam) **21**, 877 (1955)
 - [3] L. Berger, Phys. Rev. B **2**, 4559 (1970)
 - [4] R. Karplus and J. M. Luttinger, Phys. Rev. **95**, 1154 (1954); J. M. Luttinger, Phys. Rev. **112**, 739 (1958)
 - [5] M.-C. Chang and Q. Niu, Phys. Rev. B **53**, 7010 (1996); G. Sundaram and Q. Niu, *ibid.* **59**, 14915 (1999)
 - [6] T. Jungwirth, Q. Niu, and A. H. MacDonald, Phys. Rev. Lett. **88**, 207208 (2002)
 - [7] M. Onoda and N. Nagaosa, J. Phys. Soc. Jpn. **71**, 19 (2002)
 - [8] D. Xiao, M.-C. Chang, and Q. Niu, Rev. Mod. Phys. **82**, 1959 (2010)
 - [9] Y. Yao, L. Kleinman, A. H. MacDonald, J. Sinova, T. Jungwirth, D.-S. Wang, E. Wang, and Q. Niu, Phys. Rev. Lett. **92**, 037204 (2004)
 - [10] X. Wang, D. Vandervilt, J. R. Yates, and I. Souza, Phys. Rev. B **76**, 195109 (2007)
 - [11] P. N. Dheet, Phys. Rev. **156**, 637 (1967)
 - [12] T. Miyasato, N. Abe, T. Fujii, A. Asamitsu, S. Onoda, Y. Onose, N. Nagaosa, and Y. Tokura, Phys. Rev. Lett. **99**, 086602 (2007)
 - [13] Y. Tian, L. Ye, and X. F. Jin, Phys. Rev. Lett. **103**, 087206 (2009)
 - [14] J. M. Lavine, Phys. Rev. **123**, 1273 (1961)
 - [15] L. Ye, Y. Tian, X. F. Jin, and D. Xiao, arXiv:1105.5664.
 - [16] G. Y. Guo and H. H. Wang, Chin. J. Phys. **38**, 949 (2000)

- [17] G. Y. Guo, Phys. Rev. B **55**, 11619 (1997)
- [18] G. Y. Guo, W. M. Temmerman, and H. Ebert, Physica B **172**, 61 (1991)
- [19] M. S. S. Brooks, Physica B B **130**, 6 (1985)
- [20] V. I. Anisimov, J. Zaanen, and O. K. Andersen, Phys. Rev. B **44**, 943 (1991)
- [21] V. I. Anisimov, I. V. Solovyev, M. A. Korotin, M. T. Czyzyk and G. A. Sawatzky, Phys. Rev. B **48**, 16929 (1993)
- [22] M. T. Czyzyk and G. A. Sawatzky, Phys. Rev. B **49**, 14211 (1994)
- [23] I. Yang, S. Y. Savrasov, and G. Kotliar, Phys. Rev. Lett. **87**, 216405 (2001)
- [24] O. K. Andersen, Phys. Rev. B **12**, 3060 (1975)
- [25] M. Marder, Condensed Matter Physics (John Wiley, Sons, Inc., New York, 2000).
- [26] G. Y. Guo, Y. Yao, and Q. Niu, Phys. Rev. Lett. **94**, 226601 (2005)
- [27] G. Y. Guo and H. Ebert, Phys. Rev. B **51**, 12633 (1995)
- [28] P. Blaha, K. Schwarz, G. Madsen, D. Kvasnicka, and J. Luitz, *WIEN2K, An Augmented Plane Wave Local Orbitals Program for Calculating Crystal Properties* (Technische University Wien, Austria, 2002)
- [29] J. P. Perdew, K. Burke, and M. Ernzerhof, Phys. Rev. Lett. **77**, 3865 (1996)
- [30] C. Kittel, *Introduction to Solid State Physics*, Seven edition
- [31] P. E. Blöchl, O. Jepsen and O. K. Andersen, Phys. Rev. B **49**, 16223 (1994)
- [32] *Landolt-Börnstein, New Series*, Vol. III/19a, edited by H. P. J. Wein (Springer, Berlin 1988)
- [33] C. S. Wang and J. Callaway, Phys. Rev. B **9**, 4897 (1974)
- [34] D. C. Tsui, Phys. Rev. **164**, 669 (1967)
- [35] S. Lowitzer, D. Ködderitzsch, and H. Ebert, Phys. Rev. Lett. **105**, 266604 (2010)
- [36] A. A. Kovalev, J. Sinova, and Y. Tserkovnyak, Phys. Rev. Lett. **105**, 036601 (2010)
- [37] E. Roman, Y. Mokrousov, and I. Souza, Phys. Rev. Lett. **103**, 097203 (2009)
- [38] J. Kötzler and W. Gil, Phys. Rev. B **72**, 060412(R) (2005)